Heterogeneous nucleation of plastic defects and tension-compression asymmetry in the presence of vacancies in W single crystals

Ziyi Li, Wensheng Liu, Yunzhu Ma, Chaoping Liang*

National Key Laboratory of Science and Technology for High–strength Structural Materials, Central South University, Changsha 410083, China

Table Captions

Table. 1 Physical properties of tungsten from MD simulation using Zhou et al. EAM potential, first-principles (FP) calculations, and experiments.

Table. 2 Defect Formation properties (vacancy formation energy E_v^f, interstitial formation energy E_i^f and unstable stacking fault energy E_{usf}) of tungsten from MD simulation using Zhou et al. EAM potential, other potential, and first-principles (FP) calculations.

* Corresponding author: cpliang@csu.edu.cn (C.P. Liang)

Table. 1 Physical properties of tungsten from MD simulation using Zhou et al. EAM potential, first-principles (FP) calculations, and experiments.

Method	**a (Å)**	**C_{11} (GPa)**	**C_{12} (GPa)**	**C_{44} (GPa)**
MD (zhou)	3.165	522.5	204.2	160.8
FP (PBE)	3.172	520	188	141
Exp. [1]	3.165	521	202	160

Table. 2 Defect Formation properties (vacancy formation energy E_v^f, interstitial formation energy E_i^f and unstable stacking fault energy E_{usf}) of tungsten from MD simulation using Zhou et al. EAM potential, other potential, and first-principles (FP) calculations.

Method	$\boldsymbol{E_v^f}$ **(eV)**	$\boldsymbol{E_i^f}$ **(eV)**	$\boldsymbol{E_{usf}}$ $\boldsymbol{(mJ/m^2)}$
MD (zhou [2])	3.575	10.557	1725.98
MD (Marinica [3])	3.485	10.42	1502.64
FP (Marinica [3])	3.49	10.53	1686.41

Figure Captions

Fig. S1. The evolution of the elastic constants with pressure and compared with Qi's potential [4].

Fig. S2. Comparison of GSFE of tungsten in $\{112\}\langle 111\rangle$ faults with different potentials [5][6].

Fig. S3. Stress-strain curves for single crystal tungsten with different simulation cells in tension and compression at strain rate of 10^8 s^{-1} with vacancy concentrations 0.02%.

Fig. S4 Snapshots of atomistic configuration during tension deformation process ((a)ε=2.69%, (b)ε=2.74%, (c)ε=2.77%) and compression deformation process ((d)ε=−6.20%, (e)ε=−6.59%, (f)ε=−6.62%) at strain rate $10^8\ s^{-1}$ along [100] orientation for larger cell (vacancy concentration 0.02%).

Fig. S5. Comparison of total energy of tungsten for 1 fs case and 10 fs case under [100] uniaxial tension.

Fig. S6. Averaged flow stress after yielding of tungsten from MD simulation under uniaxial tension and compression along different orientations.

Fig. S7. Snapshots of atomistic configuration during tension deformation process ((a)ε=2.45%, (b)ε=2.48%, (c)ε=2.49%) and compression deformation process ((d)ε=−5.13%, (e)ε=−5.51%, (f)ε=−5.54%) at strain rate $10^8\ s^{-1}$ along [100] orientation for initial cell (vacancy concentration 1.029%).

Fig. S8. Snapshots of vacancy evolution during compression deformation process at strain rate $10^8\ s^{-1}$ along [100] orientation for initial cell (vacancy concentration 0.02%). ((a) $\varepsilon = 6.01\%$, (b) $\varepsilon = 6.03\%$, (c) $\varepsilon = 6.08\%$).

Fig. S9. The local structural evolution during compression deformation at strain rate $10^8\ s^{-1}$ along [100] orientation (vacancy concentration 0.02%).

Fig. S10. The input files to calculate the tensile and compressive loading through MD simulations.

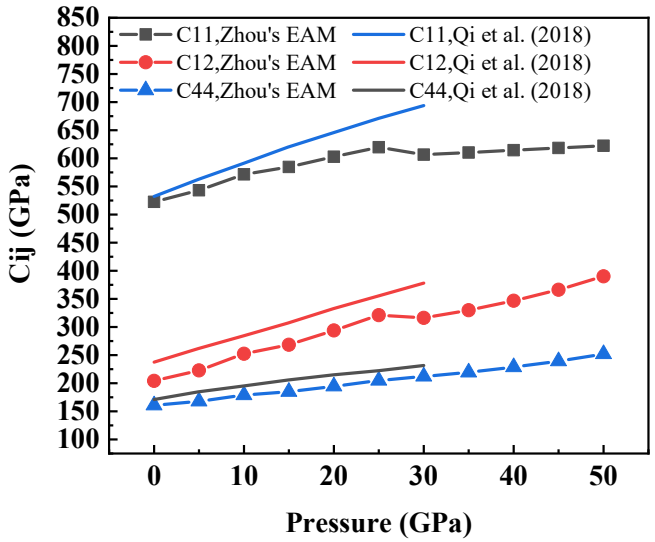

Fig. S1. The evolution of the elastic constants with pressure and compared with Qi's potential [4].

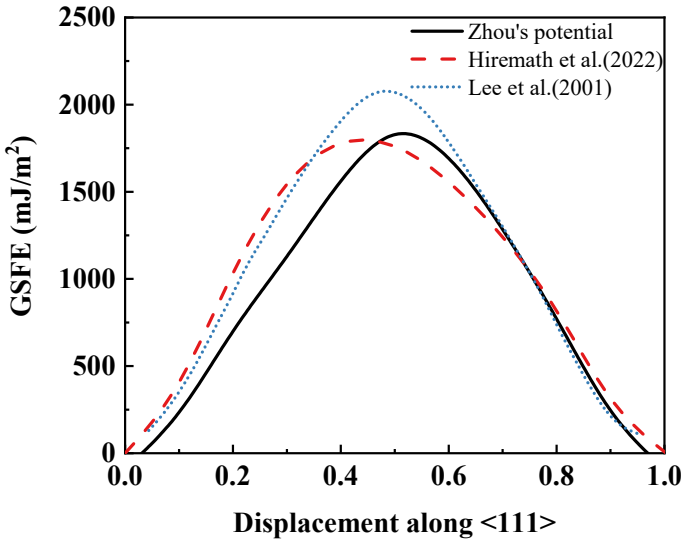

Fig. S2. Comparison of GSFE of tungsten in {112}⟨111⟩ faults with different potentials [5][6].

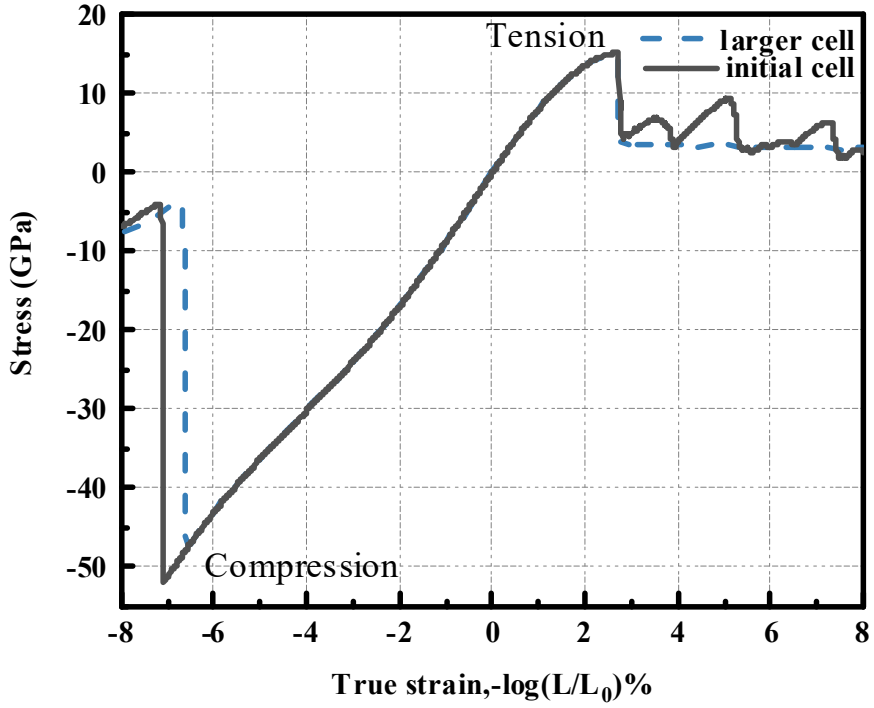

Fig. S3. Stress-strain curves for single crystal tungsten with different simulation cells in tension and compression at strain rate of 108 s-1 with vacancy concentrations 0.02%.

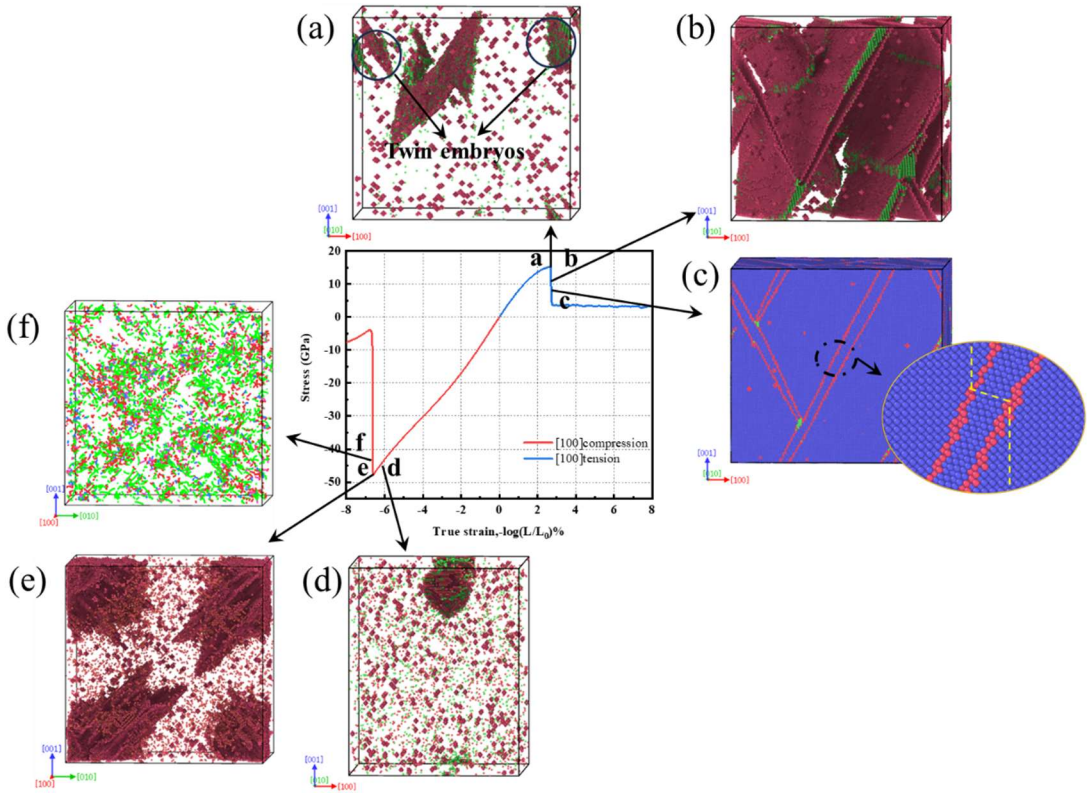

Fig. S4 Snapshots of atomistic configuration during tension deformation process ((a)ε=2.69%, (b)ε=2.74%, (c)ε=2.77%) and compression deformation process ((d)ε=−6.20%, (e)ε=−6.59%, (f)ε=−6.62%) at strain rate $10^8\,s^{-1}$ along [100] orientation for larger cell (vacancy concentration 0.02%).

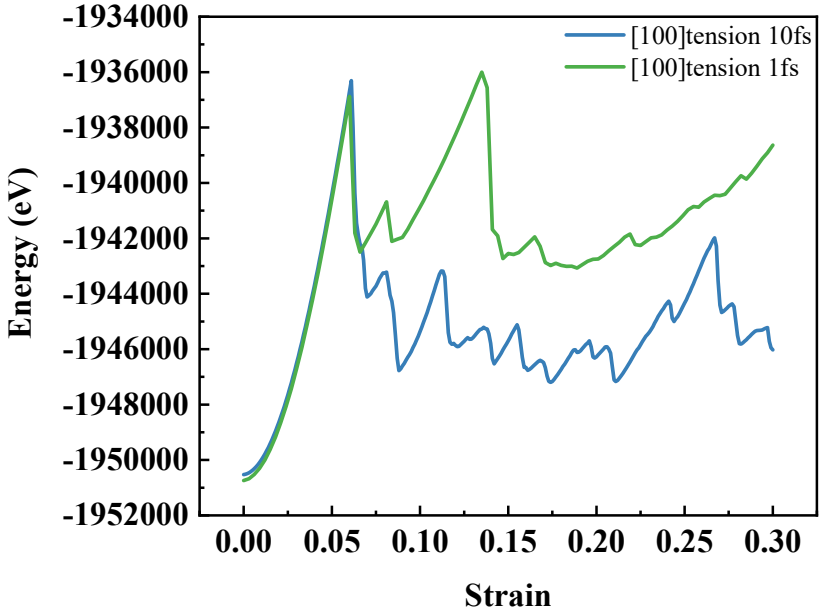

Fig. S5. Comparison of total energy of tungsten for 1 fs case and 10 fs case under [100] uniaxial tension.

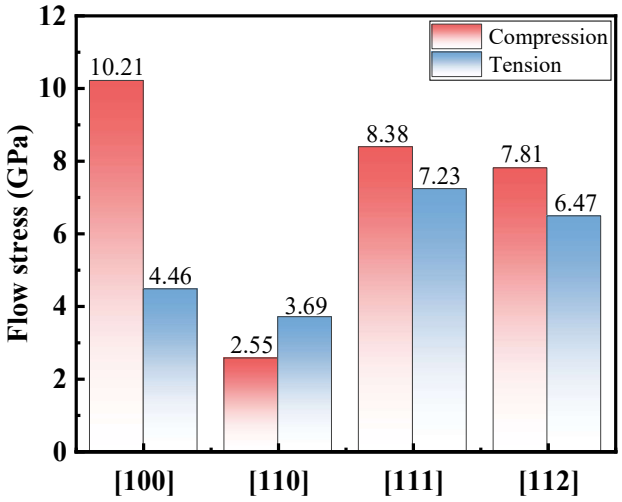

Fig. S6. Averaged flow stress after yielding of tungsten from MD simulation under uniaxial tension and compression along different orientations.

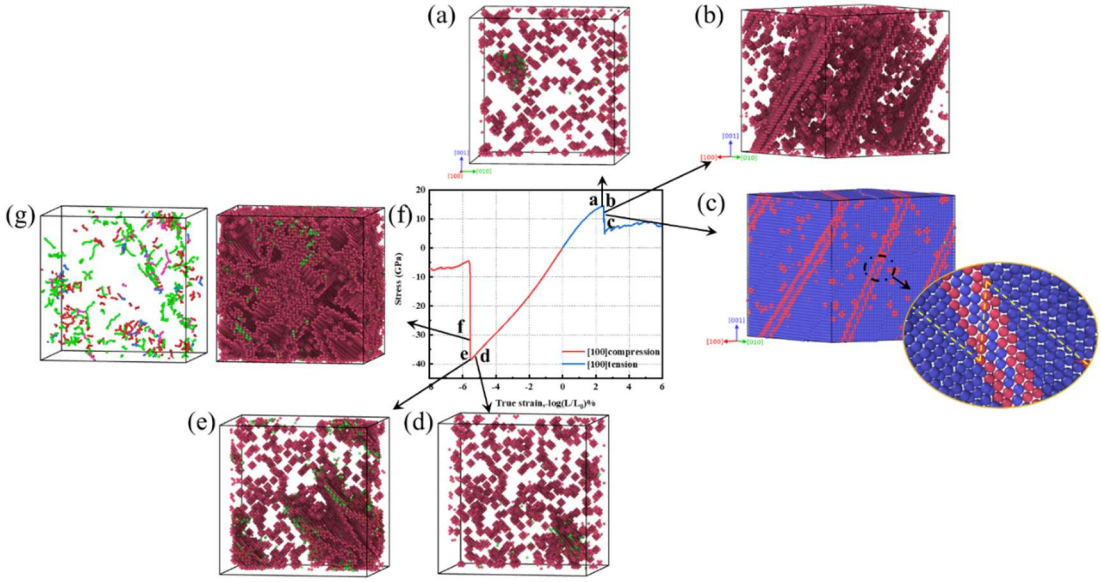

Fig. S7. Snapshots of atomistic configuration during tension deformation process ((a)ε=2.45%, (b)ε=2.48%, (c)ε=2.49%) and compression deformation process ((d)ε=−5.13%, (e)ε=−5.51%, (f)ε=−5.54%) at strain rate $10^8\ s^{-1}$ along [100] orientation for initial cell (vacancy concentration 1.029%).

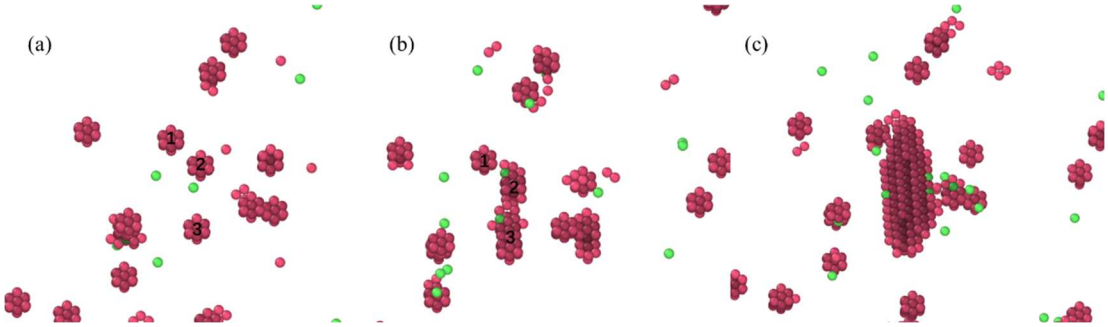

Fig. S8. Snapshots of vacancy evolution during compression deformation process at strain rate $10^8\ s^{-1}$ along [100] orientation for initial cell (vacancy concentration 0.02%). ((a) $\varepsilon = 6.01\%$, (b) $\varepsilon = 6.03\%$, (c) $\varepsilon = 6.08\%$).

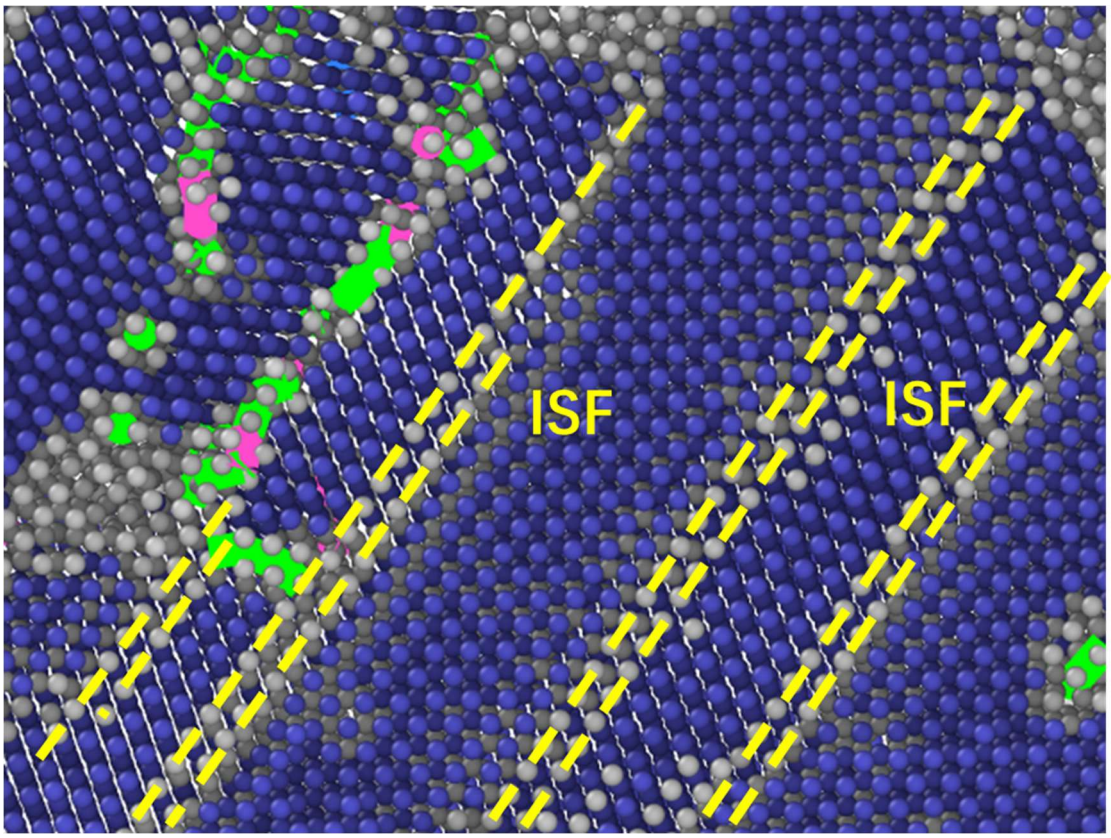

Fig. S9. The local structural evolution during compression deformation at strain rate $10^8\ s^{-1}$ along [100] orientation (vacancy concentration 0.02%)

```
# --------------- INITIALIZATION ------------------
clear
units     metal
dimension 3
boundary  p p p
atom_style  atomic
atom_modify map array

#####################################
read_data str.out

#variable minlength equal 100
variable xlen equal lx
variable ylen equal ly
variable zlen equal lz

print "lx: ${xlen}"
print "ly: ${ylen}"
print "lz: ${zlen}"


# ----------------------- FORCE FIELDS ----------------------
pair_style  eam/alloy
pair_coeff  * * WCu.eam.alloy W

#---------------------------Settings--------------------------
compute csym all centro/atom bcc
compute eng all pe/atom
compute eatoms all reduce sum c_eng
compute peratom all pe/atom

#####################################
# EQUILIBRATION
reset_timestep  0
timestep 0.001
velocity all create 300 12345 mom yes rot no
fix 1 all npt temp 300 300 1 iso 0 0 1 drag 1

# Set thermo output
thermo 1000
thermo_style custom step lx ly lz press pxx pyy pzz pe temp

# Run for at least 10 picosecond (assuming 1 fs timestep)
run 20000
unfix 1

# Store final cell length for strain calculations
variable tmp equal "lx"
variable L0 equal ${tmp}
print "Initial Length, L0: ${L0}"

#####################################
```

```
# DEFORMATION
reset_timestep  0

fix   1 all npt temp 300 300 1 y 0 0 1 z 0 0 1 drag 1
variable srate equal 1.0e8
variable srate1 equal "-v_srate / 1.0e12"
fix   2 all deform 1 x erate ${srate1} units box remap x

# Output strain and stress info to file
# for units metal, pressure is in [bars] = 100 [kPa] = 1/10000 [GPa]
# p2, p3, p4 are in GPa
variable strain equal "(v_L0-lx)/v_L0"
variable p1 equal "v_strain"
variable p2 equal "pxx/10000"
variable p3 equal "pyy/10000"
variable p4 equal "pzz/10000"
fix def1 all print 1000 "${p1} ${p2} ${p3} ${p4}" file W_comp_100.def1.txt screen no

# Use cfg for AtomEye
dump 1 all cfg 10000 dump.comp_*.cfg mass type xs ys zs c_csym c_peratom fx fy fz
dump_modify     1 element w

# Display thermo
thermo  75000
thermo_style  custom step v_strain temp v_p2 v_p3 v_p4 ke pe press

run   3000000
```

Fig. S10. The input files to calculate the tensile and compressive loading through MD simulations.

References

[1] G. Simmons, Single crystal elastic constants and calculated aggregate properties, Southern Methodist Univ Dallas Tex, 1965.

[2] X.W. Zhou, R.A. Johnson, H.N.G. Wadley, Misfit-energy-increasing dislocations in vapor-deposited CoFe/NiFe multilayers, Phys. Rev. B. 69 (2004) 144113. https://doi.org/10.1103/PhysRevB.69.144113.

[3] M.C. Marinica, L. Ventelon, M.R. Gilbert, L. Proville, S.L. Dudarev, J. Marian, G. Bencteux, F. Willaime, Interatomic potentials for modelling radiation defects and dislocations in tungsten, J. Phys. Condens. Matter. 25 (2013). https://doi.org/10.1088/0953-8984/25/39/395502.

[4] X. Qi, N. Cai, T. Chen, S. Wang, B. Li, Experimental and theoretical studies on the elasticity of tungsten to 13 GPa, J. Appl. Phys. 124 (2018). https://doi.org/10.1063/1.5044519.

[5] M.I. Baskes, B.J. Lee, H. Kim, Y. Koo Cho, Second nearest-neighbor modified embedded atom method potentials for bcc transition metals, Phys. Rev. B - Condens. Matter Mater. Phys. 64 (2001). https://doi.org/10.1103/PhysRevB.64.184102.

[6] P. Hiremath, S. Melin, E. Bitzek, P.A.T. Olsson, Effects of interatomic potential on fracture behaviour in single- and bicrystalline tungsten, Comput. Mater. Sci. 207 (2022) 111283. https://doi.org/10.1016/j.commatsci.2022.111283.